

TABLE 1. Small Magellanic Cloud periphery carbon stars

Name	id field	RA	(1950)	Dec	ℓ	b	v_{helio}	v_{gc}	Q	n	R	$B_j - R$	comments
C0142-7219	029-010	1 42	03.7	-72 19 48	318.1	-39.8	122.0	-9.2	7	1	15.4	3.45	
C0136-7239	029-023	1 36	16.6	-72 39 55	298.1	-44.2	173.3	15.5	7	2	16.0	3.17	
C0141-7243	029-031	1 41	51.3	-72 43 52	297.5	-44.0	144.4	-14.6	7	1	15.6	2.53	
C0142-7251	029-035	1 42	48.4	-72 51 48	297.5	-43.9	128.9	-30.4	7	2	15.6	4.53	
C0137-7257	029-039	1 37	42.9	-72 57 20	298.0	-43.9	166.6	7.9	7	1	15.6	3.41	
C0134-7301	029-040	1 34	55.7	-73 01 29	298.3	-43.9	174.3	16.0	7	1	15.8	2.90	
C0130-7312	029-048	1 30	32.7	-73 12 55	298.5	-43.7	125.9	-32.6	7	1	15.7	2.94	
C0135-7331	029-066	1 35	11.3	-73 31 33	298.5	-43.4	129.8	-29.4	7	1	15.6	4.10	
C0144-7347	029-098	1 44	04.1	-73 47 18	297.7	-43.0	125.1	-36.1	7	1	15.4	2.82	
C0143-7356	029-110	1 43	59.1	-73 56 03	297.8	-42.8	184.7	23.0	7	1	15.6	2.72	
C0141-7403	029-123	1 41	53.1	-74 03 16	298.0	-42.7	164.6	2.9	7	1	15.9	2.65	
C0134-7505	029-218	1 34	26.4	-75 05 26	299.0	-41.9	131.9	-30.3	7	1	15.6	2.95	
C0118-7521	029-232	1 18	04.6	-75 21 11	300.5	-41.8	150.5	-9.8	7	1	15.6	2.99	
C0117-7539	029-243	1 17	09.5	-75 39 46	300.6	-41.5	156.0	-4.8	7	1	16.3	2.93	
C0149-7525	029-244	1 49	33.3	-75 25 53	298.0	-41.3	137.9	-27.1	7	1	16.8	3.99	
C0020-7527	029-247	0 20	39.6	-75 27 13	305.3	-41.7	140.8	-12.1	7	1	15.0	3.33	
C0130-7554	029-259	1 30	34.5	-75 54 26	299.6	-41.1	158.4	-4.8	7	1	15.3	2.61	
C0142-7549	029-261	1 42	49.9	-75 49 23	298.6	-41.0	125.2	-39.6	7	1	15.8	3.69	
C0118-7559	029-263	1 18	12.4	-75 59 57	300.6	-41.2	150.9	-10.6	7	1	16.4	4.03	
C0057-7603	029-265	0 57	03.5	-76 03 11	306.8	-40.9	184.3	32.2	7	1	16.3	2.57	
C0055-7603	029-267	0 55	59.7	-76 03 14	302.4	-41.2	169.5	10.6	7	1	15.8	2.46	
C0058-7613	029-268	0 58	33.2	-76 13 01	304.2	-41.1	149.9	-6.2	7	1	15.7	4.59	
C0138-7609	029-270	1 38	56.7	-76 09 24	299.0	-40.8	151.6	-13.1	7	1	15.6	2.43	
C0050-7635	029-278	0 50	15.6	-76 35 17	302.8	-40.7	165.8	6.5	7	1	15.6	2.69	
C0055-7644	029-279	0 55	17.5	-76 44 35	302.5	-40.6	187.4	27.4	7	1	16.2	2.44	
C0036-7650	029-282	0 36	30.9	-76 50 03	303.9	-40.4	138.0	-20.1	7	1	15.4	2.68	
C0141-7731	029-289	1 41	04.3	-77 31 55	299.3	-39.4	134.5	-33.0	5	1	15.4	2.61	M
C0102-7749	029-290	1 02	15.2	-77 49 38	302.1	-39.5	216.0	60.5	7	1	15.8	2.72	
C0155-7238	030-02	1 55	21.0	-72 38 13	296.2	-43.8	97.8	-63.3	7	1	15.6	3.83	
C0154-7238	030-03	1 54	11.7	-72 38 53	296.3	-43.8	125.7	-35.3	7	1	14.8	2.80	
C0151-7306	030-09	1 51	02.1	-73 06 54	296.8	-43.4	158.4	-3.0	7	1	14.8	2.88	
C0132-7309	030-11	1 32	23.2	-73 09 30	298.6	-43.8	172.7	14.5	7	1	15.5	3.17	
C0155-7343	030-15	1 55	29.4	-73 43 16	296.7	-42.8	151.2	-11.8	7	1	15.8	3.31	
C0149-7354	030-18	1 49	56.2	-73 54 03	297.3	-42.8	107.1	-37.5	7	1	15.3	2.47	bad coords
C0133-7351	030-23	1 33	41.7	-73 51 38	298.7	-43.1	122.1	-37.6	6	1	16.3	2.70	
C0148-7403	030-24	1 48	47.2	-74 03 32	297.4	-42.6	153.6	-9.0	7	1	16.3	3.17	
C0135-7356	030-25	1 35	08.1	-73 56 40	298.6	-43.0	153.6	-6.5	7	1	15.0	2.83	
C0139-7406	030-29	1 39	20.0	-74 06 46	298.3	-42.7	188.4	27.1	4	1	16.9	4.35	wk C
C0147-7437	030-34	1 47	18.4	-74 37 33	297.8	-42.1	151.1	-12.2	7	1	15.1	2.80	
C0131-7447	030-36	1 31	25.2	-74 47 31	299.2	-42.2	183.1	21.8	5	1	14.7	2.58	wk C
C0127-7452	030-37	1 27	49.7	-74 52 03	299.5	-42.2	139.1	-21.6	7	1	14.5	2.94	
C0154-7508	030-38	1 54	50.3	-75 08 26	297.4	-41.4	126.4	-39.1	7	1	15.1	3.65	
C0208-7515	030-40	2 08	23.8	-75 15 23	296.4	-41.0	134.1	-33.7	7	1	15.1	2.89	
C0131-7505	030-42	1 31	42.3	-75 05 26	299.3	-42.0	121.9	-39.6	7	1	15.2	2.64	
C0127-7503	030-43	1 27	26.0	-75 03 02	299.6	-42.0	173.7	12.5	5	1	16.0	2.50	
C0201-7536	030-44	2 01	28.5	-75 36 10	297.1	-40.9	130.5	-36.6	6	1	15.0	2.48	flat sp.
C0143-7558	030-47	1 43	22.0	-75 58 39	298.6	-40.9	164.8	-0.3	7	1	14.7	2.61	
C0105-6810	051-08	1 05	53.4	-68 10 34	300.5	-49.0	139.6	-2.7	7	2	14.9	3.16	

TABLE 1. (continued)

Name	id field	RA	(1950)	Dec	ℓ	b	v_{helio}	v_{gc}	Q	n	R	$B_j - R$	comments
C0100-6845	051-14	1 00	20.0	-68 45 21	301.4	-48.5	143.2	0.8	7	1	15.2	2.43	
C0055-6847	051-15	0 55	32.5	-68 47 54	302.0	-48.5	93.8	-47.7	7	1	15.3	2.76	
C0059-6849	051-16	0 59	53.2	-68 49 23	301.5	-48.4	64.6	-77.9	7	1	15.6	2.54	
C0049-6914	051-24	0 49	21.8	-69 14 29	302.9	-48.1	183.3	41.9	7	1	15.5	3.31	
C0122-6910	051-26	1 22	27.0	-69 10 32	298.5	-47.8	164.7	16.7	7	1	15.2	2.87	
C0047-6942	051-31	0 47	28.5	-69 42 40	303.1	-47.6	137.2	-5.1	7	1	15.4	3.06	
C0036-6954	051-32	0 36	33.0	-69 54 12	304.5	-47.4	151.2	10.3	7	1	15.5	2.56	
C0115-6954	051-33	1 15	43.6	-69 54 30	299.6	-47.2	94.6	-53.5	7	1	15.4	3.55	
C0116-7003	051-35	1 16	00.9	-70 03 25	299.6	-47.1	156.6	8.1	7	1	16.0	2.62	
C0107-7012	051-40	1 07	39.0	-70 12 58	300.6	-47.0	115.7	-31.6	7	1	15.3	2.88	
C0115-7036	051-55	1 15	49.8	-70 36 23	299.7	-46.5	164.2	14.3	7	1	15.5	2.50	
C0124-7105	051-73	1 24	13.6	-71 05 09	298.8	-46.0	168.7	16.3	4	1	15.2	2.83	weak C
C0124-7106	051-76	1 24	52.6	-71 06 11	298.8	-46.0	115.3	-37.0	7	1	15.3	2.42	
C0124-6758	052-04	1 24	26.7	-67 58 33	298.0	-49.1	206.2	61.0	7	1	15.8	2.79	
C0134-6828	052-06	1 34	31.3	-68 28 36	296.7	-48.3	109.7	-39.0	7	3	15.9	3.25	
C0112-6825	052-08	1 12	45.8	-68 25 07	299.6	-48.7	157.2	13.0	7	1	15.9	2.57	
C0126-6840	052-09	1 26	18.5	-68 40 53	297.9	-48.2	97.5	-50.1	2	1	15.8	2.55	C (thru clouds)
C0117-6848	052-10	1 17	06.3	-68 48 08	299.1	-48.3	119.2	-26.6	7	3	15.0	3.60	
C0116-6856	052-11	1 16	07.8	-68 56 23	299.3	-48.2	-173.4	319.3	0	1	15.3	2.58	clouds; vy. ft.
C0121-6923	052-12	1 21	45.9	-69 23 49	298.7	-47.6	136.2	-12.0	6	1	15.9	4.11	
C0110-6932	052-13	1 10	46.9	-69 32 52	300.1	-47.6	132.9	-13.5	6	1	15.9	3.14	
C0127-6842	052-14	1 27	15.2	-69 42 26	298.1	-47.2	209.3	59.2	7	1	15.8	2.65	
C0132-6956	052-16	1 32	30.0	-69 56 22	297.5	-46.9	98.8	-52.7	7	1	15.6	3.97	
C0110-6957	052-17	1 10	02.4	-69 57 05	300.3	-47.2	158.0	10.7	4	1	16.6	3.12	faint sp.
C0118-7004	052-18	1 18	34.1	-70 04 03	299.2	-47.0	460.6	311.3	0	1	15.3	2.57	C; clouds ft.
C0120-7028	052-22	1 20	18.1	-70 28 10	299.1	-46.6	147.4	-2.9	7	1	16.6	3.44	
C0217-7020	052-21	2 17	16.1	-70 20 33	292.6	-45.1	141.8	-20.0	1	1	16.4	2.60	too ft. cloudy
C0109-7022	052-23	1 09	41.4	-70 22 02	300.4	-46.8	114.6	-33.5	7	1	15.4	4.49	
C0217-7023	052-24	2 17	03.8	-70 23 16	292.6	-45.2	549.7	388.1	0	1	17.1	2.60	M
C0124-7056	052-29	1 24	32.4	-70 56 00	298.8	-46.1	108.4	-43.6	7	1	14.9	2.71	
C0116-7058	052-30	1 16	15.5	-70 58 53	298.1	-44.2	168.2	10.4	7	1	15.5	2.77	
C0125-7121	052-31	1 25	14.9	-71 21 24	299.0	-45.7	97.5	-55.3	7	1	15.4	3.08	
C0123-7137	052-33	1 23	00.4	-71 37 09	299.1	-45.4	109.2	-44.2	7	1	15.2	2.98	
C0144-7145	052-35	1 44	25.3	-71 45 28	296.9	-44.9	132.1	-25.4	7	1	14.2	2.90	
C0124-7146	052-36	1 24	45.0	-71 46 17	299.0	-45.3	120.9	-32.9	7	1	15.3	2.70	
C0117-7143	052-37	1 17	40.0	-71 43 13	299.7	-45.4	102.5	-50.1	7	1	15.1	3.04	
C0123-7148	052-38	1 23	27.5	-71 48 03	299.1	-45.2	120.4	-33.5	7	1	15.9	2.89	
C0132-7205	052-39	1 32	39.5	-72 05 06	298.2	-44.8	169.8	13.6	7	1	15.6	2.97	
C0131-7211	052-41	1 31	18.8	-72 11 53	298.4	-44.7	118.9	-37.2	7	1	15.3	2.90	
C0148-7213	052-42	1 48	38.2	-72 13 54	296.6	-44.3	116.8	-42.6	7	1	15.0	3.70	
C0120-7234	052-45	1 20	03.7	-72 34 33	299.7	-44.5	118.0	-36.9	7	1	15.8	4.15	
C0154-7238	052-46	1 54	11.8	-72 38 54	296.3	-43.8	127.3	-33.7	7	1	15.2	2.81	
C0118-7246	052-49	1 18	52.9	-72 46 05	299.8	-44.4	132.2	-22.8	7	1	15.3	3.45	
C0228-7045	053-3	2 28	51.0	-70 45 25	291.7	-44.4	162.8	-1.3	7	4	15.1	2.94	
C0108-6743	080-07	1 08	28.3	-67 43 46	300.1	-49.5	130.9	-10.5	7	1	17.1	3.44	
RAW-1694		1 18	39.1	-72 58 46	300.0	-44.1	173.1	17.6	7	1	17.1		
RAW-1695		1 18	42.9	-72 41 31	299.9	-44.4	149.4	-5.4	7	1	16.9		
RAW-1696		1 18	52.9	-72 46 06	299.9	-44.3	142.9	-12.2	7	1	16.4		

TABLE 1. (continued)

Name	id field	RA	(1950)	Dec	ℓ	b	v_{helio}	v_{gc}	Q	n	R	$B_j - R$	comments
RAW-1697		1 19 08.1	-73 13 19	300.0	-43.9	145.4	-10.5	7	1	17.3			
RAW-1698		1 19 13.7	-72 52 03	299.8	-44.2	182.6	27.0	7	1	17.7			
RAW-1699		1 19 22.6	-73 09 44	299.9	-44.0	143.2	-12.6	7	1	17.1			
RAW-1700		1 20 21.3	-72 44 43	299.7	-44.4	148.1	-7.0	6	1	17.6			
RAW-1701		1 20 23.1	-72 37 39	299.7	-44.5	191.2	36.2	7	1	17.0			
RAW-1702		1 20 24.9	-72 58 10	299.7	-44.1	123.2	-32.7	7	1	17.0			
RAW-1703		1 20 29.2	-73 15 24	299.8	-43.8	133.5	-23.0	7	1	17.3			
RAW-1704		1 20 30.3	-72 58 26	299.7	-44.1	162.4	6.4	7	1	17.3			
RAW-1705		1 20 57.5	-72 57 00	299.7	-44.1	119.0	-36.9	7	1	16.3			
RAW-1706		1 21 14.0	-73 01 41	299.7	-44.1	160.5	4.5	7	1	16.3			
RAW-1707		1 21 55.6	-73 21 58	299.7	-43.7	124.3	-32.5	7	1	16.5			

Submitted to the Astronomical Journal

Magellanic Cloud Periphery Carbon Stars IV: The SMC

William E. Kunkel

Carnegie Institution of Washington, La Serena, Chile

kunkel@jeito.lco.cl

Serge Demers

Département de Physique Université de Montréal, Montreal, Qc H3C 3J7, Canada

demers@astro.umontreal.ca

and

M. J. Irwin

Institute of Astronomy, Cambridge CB3 0HA, England

mike@mail.ast.cam.ac.uk

ABSTRACT

The kinematics of 150 carbon stars observed at moderate dispersion on the periphery of the Small Magellanic Cloud are compared with the motions of neutral hydrogen and early type stars in the Inter-Cloud region. The distribution of radial velocities implies a configuration of these stars as a sheet inclined at 73 ± 4 degrees to the plane of the sky. The near side, to the South, is dominated by a stellar component; to the North, the far side contains fewer carbon stars, and is dominated by the neutral gas. The upper velocity envelope of the stars is closely the same as that of the gas. This configuration is shown to be consistent with the known extension of the SMC along the line of sight, and is attributed to a tidally induced disruption of the SMC that originated in a close encounter with the LMC some 0.3 to 0.4 Gyr ago. The dearth of gas on the near side of the sheet is attributed to ablation processes akin to those inferred by Weiner & Williams (1996) to collisional excitation of the leading edges of Magellanic Stream clouds. Comparison with kinematic data of Hardy, Suntzeff & Azzopardi (1989), Maurice *et al.* (1989), and Mathewson *et al.* (1986, 1988) leaves little doubt that forces other than gravity play a role in the dynamics of the H I.

Subject headings: carbon stars, Magellanic Clouds, galaxies: interactions

1. INTRODUCTION

The discovery of the Magellanic Stream by Wannier & Wrixon (1972) suggested to many that an interaction between the Magellanic Clouds had occurred in the relatively recent past, and the more detailed observations of the Stream by Mathewson and his co-workers (Mathewson, Schwarz & Murray 1977, Mathewson & Ford 1984) revealed a structure as though a turbulent wake had broken the debris into six distinct fragments, extending over 110° on the sky. Attempts to account for the observations led to both purely tidal scenarios (Fujimoto & Sofue 1976, 1977, Davies & Wright 1977, Kunkel 1979, Murai & Fujimoto 1980) as well as others, involving ram pressure (Fujimoto & Sofue 1976, 1977, Lin & Lynden-Bell 1977, Mathewson *et al.* 1987). In these scenarios the SMC is seen to be the source of the dispersed gas. Early theoretical investigations using N-body simulations employed fixed potentials and no gas dynamics, and met with limited success. No simulation proved able to deal with the absence of a stellar component in the resulting debris stream (Moore & Davis 1994). By 1976 interpretations involving stars appeared. Kunkel & Demers (1976), and independently Lynden-Bell (1976) noted that the alignment of the Stream with the distribution of dwarf spheroidal satellites of the Milky Way followed a great circle on the sky within some ten degrees, leading to the inference that a close encounter of the Magellanic Clouds with the Galaxy had stripped debris fragments in the current form of dwarf spheroidal galaxies from the Clouds well after their initial formation, in the manner described by Alar and Yuri Toomre (1972). Kunkel (1979) suggested that the difficulty in creating a trailing tail without a leading bridge, and further, to explain the absence of stars in the stream, required an early disruption, perhaps 6 Gyr ago, before star formation had advanced significantly, well prior to the current encounter between the Clouds and the Galaxy. Such an event would then create gaseous configurations loosely bound to the Clouds until the present. Within a year the difficulty presented by the “tail-only” scenario was elegantly resolved by Murai & Fujimoto (1980) who proposed that the binary character of the Clouds had created a debris fragment torn from the SMC perhaps 1.5 Gyr ago, during an encounter with the LMC, which then remained trapped in their joint potential well until the recent encounter with the Milky Way deposited the fragment into the tail trailing both Clouds, while the bridge locus, containing no corresponding fragment, remained unoccupied. The next observational insight came from an investigation of cepheid variables in the SMC by Mathewson, Ford, & Visvanathan (1986, 1988). Their work showed that, unlike the LMC, the depth along the line of sight of the SMC Cepheids exceeded the SMC tidal diameter, extending to tens of kpc. Although this interpretation was later challenged (Welch *et al.* 1987), evidence for an unusual extent of the SMC in the line of sight became apparent in photometry of the red giant clump (Hatzidimitriou & Hawkins 1989, Mateo and Hatzidimitriou 1992). In their photometry the extent of the SMC was seen to vary from a maximum of 23 kpc toward the NE (ESO/SERC field 52) to as little as 10 kpc in the SW (ESO/SERC field 28). More recently Hatzidimitriou, Cannon, & Hawkins (1993) found a gradient in radial velocity associated with the vertical spread in the magnitudes of the red giant clump some three degrees East of the SMC, thereby confirming the expansion of this portion of the SMC, and a start time corresponding to the epoch earlier workers had associated with the tidal encounter between the Clouds. They confirmed that this extension of stars in the line of sight ranges over

more than 15 kpc, and an expansion with a velocity gradient of 7 km s^{-1} per kpc.

A search for stellar components of the inter-cloud region (ICR) began with a survey by West-erlund & Glaspey (1971) who found a young stellar population some 5° to the East of the SMC photocenter (at $l, b = 302.8^\circ, -44.3^\circ$). Some ten years later Kunkel (1980) demonstrated the existence of a young population of stars associated with the denser ensembles of neutral hydrogen 8° to the East of the SMC. In the following decade a complete Schmidt survey revealed that the entire ICR extending all the way to the LMC was covered with a thin population of young stars of surprisingly uniform age (Demers & Irwin 1991). All the blue stars of the ICR were found to be unexpectedly young, much younger than the time scale attributed to the interaction event between the two Clouds (Grondin *et al.* 1992). The presence of an old stellar component in the ICR, older than its dynamical time scale, was found at about this time, in the form of carbon stars that likewise extended over the entire ICR (Demers, Irwin & Kunkel 1993, hereafter Paper I). Some years before the survey of the periphery carbon stars was completed, an early assessment of the ICR data then available suggested that the ratio of neutral gas to carbon stars, examined as a function of radial velocity (and hence distance by virtue of the expansion gradient found by Hatzidimitriou *et al.* (1993)) declines with decreasing radial velocity. Consequently carbon stars were found to dominate at the lower velocities, corresponding to the bridge, while H I dominates the tail which shows primarily the more positive velocities (Kunkel, Demers & Irwin 1995). This interpretation is the first indication that non-gravitational forces may play a non-negligible role in the ICR dynamics.

The study reported here completes the survey of carbon stars over the entire periphery of the SMC, and augments the interpretive portion of our analysis with the extensive kinematic observations of Hatzidimitriou *et al.* (1997). Section 2 describes our observational material and the procedures employed to produce it, Section 3 describes briefly the material incorporated from other sources, while section 4 presents the data in a variety of geometric projections selected to facilitate interpretations. Section 5 provides a description of an interpretive scenario based on self-gravitating N-particle simulations modeled on a disruptive interaction with the LMC, from which interpretive constraints are inferred. Last, in the light of insights drawn from the simulations, section 6 examines interpretive options relating the new observations of carbon star kinematics to data for other classes of objects, principally the neutral hydrogen, and from these, explores alternative scenarios for non-gravitational dynamical processes affecting the tidal interpretation in the line of sight. The study ends with an exploration of some astronomical implications.

2. OBSERVATIONS

The observations were obtained between 1991 and 1997 with the modular spectrograph at the duPont 2.5 meter telescope during 42 observing nights, the preponderant majority of the data being taken at a resolution FWHM of 1.1\AA over a spectral region between 7850 and 8760\AA , reported earlier (Kunkel, Demers & Irwin 1997, hereafter Paper II). Apart from two initial survey fields selected

especially for the original discovery mission, the complete SMC survey searched 12 ESO/SERC fields: 13, 14, 28, 29, 30, 31, 50, 51, 52, 53, 79, and 80, with kinematic data for a total of 150 carbon stars redder than $(B_j - R_f) = 2.4$. Some material not published in the earlier list is here included in an appendix. The data processing consisted in the extraction of one-dimensional spectra employing the traditional IRAF data reduction packages. After numerous trials with a variety of other template spectra, cross-correlation algorithm matching a radial velocity template derived from the R-type carbon star HD16115 with a heliocentric radial velocity of 14.0 km s^{-1} (McClure *et al.* 1985) was found to give the most satisfactory reduction of the entire data set. The master template was masked to employ three separate spectral regions known to be almost entirely free of telluric features. Two regions covered the CN bands at 7915 and 8165Å, avoiding the strong telluric water features near 8165Å, and a third region covering the Ca II triplet between 8550 and 8710Å. Comparison exposures of an argon lamp were taken after each spectrum, to assure that velocity errors arising from instrumental flexure could be held to less than 2 km s^{-1} .

Most of the spectra, logarithmically re-sampled, attained a raw signal to noise ratio of eight or more. These produced radial velocity estimates that repeated reliably, and for those stars believed to be free of binary orbital motion, to within 5 km s^{-1} of their mean (see Kunkel, Demers & Irwin (1997) for details). Increasing the instrumental dispersion yielded no improvement in the velocity precision, and we believe that the limiting precision reflects the atmospheric motions in these late type atmospheres, as had already been noted in the spectrographic data obtained for long period variables (Hughes, Wood, & Reid 1991).

To assure a proper match of the instrumental velocity system between the various nights, as well as between data obtained by other observers, 6 or more carbon stars were re-observed on most nights, and additional carbon stars were included to permit comparison with the extensive observations of Hardy, Suntzeff & Azzopardi (1989). Likewise 16 carbon stars were observed in 5 LMC globular clusters for which radial velocity measures had been obtained by Olszewski *et al.* (1991), and 7 stars in 4 SMC clusters for which velocities have been reported by Da Costa & Hatzidimitriou (1998). Since SMC and LMC candidates were observed on the same nights, the velocity systems for our data are the same for both Clouds. Stars the velocities of which appeared to deviate exceptionally from the population mean were re-observed during several observing seasons to confirm their exceptional values, or to justify their rejection as radial velocity variables.

3. SUPPLEMENTARY DATA

3.1. Carbon stars

Although our data cover the outer periphery of the SMC completely, we have supplemented the inner portion of the SMC with data taken from the lists of Hatzidimitriou *et al.* (1997) that provides velocities for 72 stars, of which there are 19 in common with our survey. The small proportion of common detections is due to different detection criteria employed by those authors, resulting in the

inclusion of a number of hotter carbon stars than the threshold adopted for our work. An offset of $+9 \text{ km s}^{-1}$ must be added to our data to bring them into line with Hatzidimitriou *et al.* (1998). We included 6 stars from the list of Hardy, Suntzeff & Azzopardi (1989) in the entire observing program for the purpose of matching our and their kinematic data. Jointly this combination forms the data set analyzed in the remainder of this paper. An offset of $+7 \text{ km s}^{-1}$ added to our data bring them into line with those of Hardy, Suntzeff & Azzopardi (1989). An offset of $+5 \text{ km s}^{-1}$ added to our data brings our data into line with the cluster data of Olszewski et al (1991); 16 stars in these clusters (NGC1751, NGC1783, NGC1806, NGC1846, and NGC2213) were observed during the program covering the SMC carbon stars.

3.2. Globular clusters

Radial velocity data for seven globular clusters are taken from the investigation of Da Costa & Hatzidimitriou (1998) to which an offset of $+18 \text{ km s}^{-1}$ has been added to bring them into line with the two objects in common with our data.

3.3. Early type stars

Spectroscopy of early type stars is from Grondin, Demers, & Irwin (1992), covering ESO/SERC fields 31, 32, and 53. Radial velocities are taken from the same source. Distances to the associations of early type were taken from B , V photometry of Demers & Battinelli (1998).

3.4. Neutral hydrogen

Although a number of newer surveys covering the neutral hydrogen distribution in the ICR are becoming available (for example Putnam *et al.* 1998), we have relied on the survey of McGee & Newton (1986) primarily to take advantage of the smoothing inherent in the lower beam resolution used. The numerical data we abstract employs all Gaussian peaks in their Table 4 greater than $3.5 \times 10^{19} \text{ cm}^{-2}$

4. PROJECTION OF THE DATA

An interpretation of the data is facilitated through specialized projections of the observational data. A schematic representation of the orientation of the orbital plane of the SMC with respect to the SMC/LMC barycenter is depicted in Figure 1, lying nearly on the observer’s line of sight.

A map of the observational data points projected on the plane of the sky is shown in Figure 2, with triangles, squares, and stars representing carbon stars, globular clusters, and stars of early

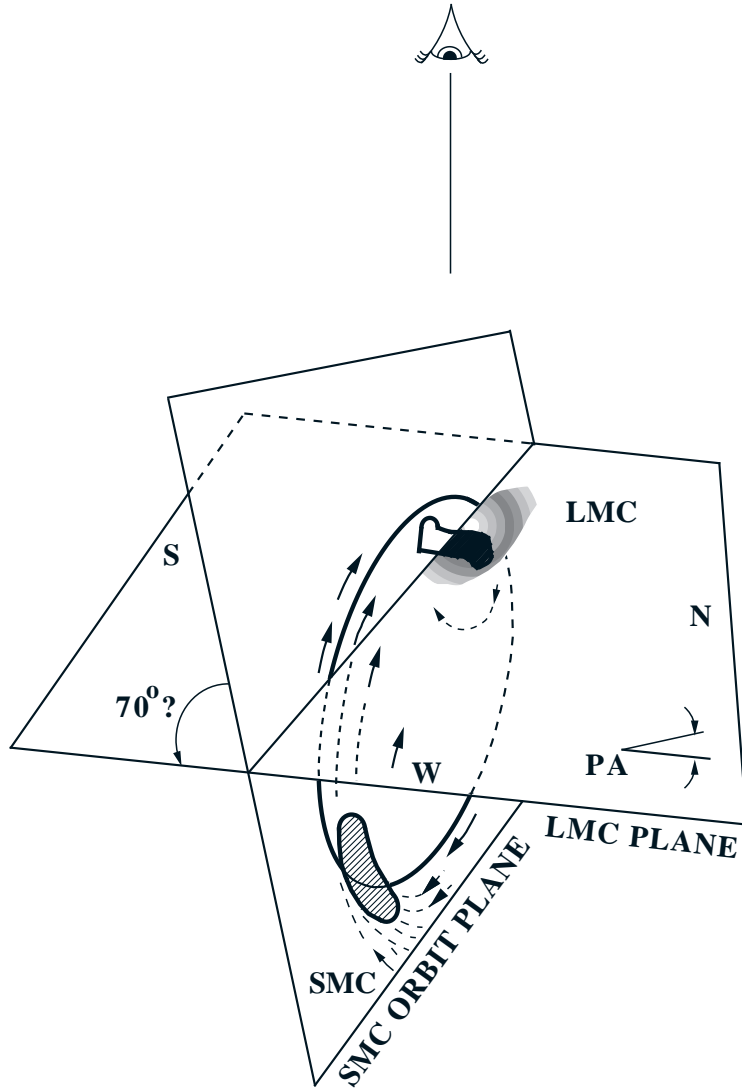


Fig. 1.— Schematic of the LMC disk plane and the SMC orbital plane about the LMC. Celestial North is to the right, West is toward the reader. The SMC orbital plane is inclined by 17° to the line of sight, with the edge nearer the observer lying southward. In this configuration the LMC rotates clockwise, and the SMC moved upward in its orbit, through the LMC plane toward the observer. Short arrows show velocities of representative debris particles.

spectral type, respectively. Two “clusters” of tiny open circles near the center of the SMC represent the carbon stars observed by Hardy, Suntzeff & Azzopardi (1989) that form a reference population with which our periphery objects are compared. Their role in this investigation will become apparent in section 6. Completeness in the carbon star data coverage extends to a radius of 12° for the carbon stars, and is less for the stars of early type, surveyed in but three ICR Schmidt fields between the Clouds. It is also less for all of the supplementary data utilized. Before the observed radial velocities can be employed in dynamical interpretation it is important to note that a component of proper motion of the SMC in the plane of the sky entails a component of velocity along the line of sight that varies with the apparent longitude in the SMC’s orbit, following the manner first described by Feitzinger et al (1977). Radial velocities employed in the analysis described below have been adjusted in this sense, assuming a proper motion parallel to that of the LMC, but less by some 60 km s^{-1} (Irwin *et al.* 1996). From the proper motion measured in our study of the LMC carbon stars (Kunkel *et al.* 1997, hereafter Paper III) we adopt a value of 180 km s^{-1} at $\text{PA}(l, b) = 310^\circ$.

The anomalous distribution of objects on the periphery of the SMC is readily apparent in figure 3, which shows a “panoramic” display of the distribution within annular zones in five ranges of radii, centered on the photocenter of the SMC (at $l, b = 302.8^\circ, -44.3^\circ$), as a function of position angle (zero toward the North Galactic pole). From the bottom toward the top the 5 zones lie between radii of 3, 4, 5, 7, 10, and 14 degrees, and as many kpc at the adopted distance of the SMC. The areas covered by the annular zones are approximately 16, 28, 75, 150, and 300 square degrees of sky. The direction toward the center of the LMC is toward $\text{PA} = 294.5^\circ$; the celestial North pole lies toward $\text{PA} = 182^\circ$. East is toward $\text{PA} = 272^\circ$. The lowest of the 5 annular zones shows a fairly uniform distribution of carbon stars, with no measurable component of rotation. Open circles between 200° and 320° of PA represent H I samples from McGee & Newton (1986), the smallest symbols corresponding to $3 \times 10^{19} \text{ cm}^{-2}$, and the largest $80 \times 10^{19} \text{ cm}^{-2}$. As we range outward beyond 4 kpc the second panel from the bottom shows a tendency for carbon stars to thin out in the PA range between 320° and 80° , to the SW of the SMC, and opposite of the direction toward the LMC. At radii beyond 5° , carbon stars are found primarily to the East of the SMC, with a slight preference southward of the line toward the LMC. At larger radii carbon stars are seen concentrated along a line directed toward the LMC (toward $\text{PA} = 295^\circ$). In the outermost zone a group of 9 ICR carbon stars group within the range $292^\circ < \text{PA} < 320^\circ$; two additional carbon stars at lesser PA’s are most likely unrelated interlopers one expects from the field density reported by Totten & Irwin (1998). The trend concentrating ICR carbon stars toward the great circle connecting the Magellanic Clouds, as well as the decrease in density (count per square degree) at larger separation from the SMC, we interpret as demonstrating the SMC to be the origin of the ICR carbon stars, rather than the LMC.

The upper three panels of Figure 3, expanding the view toward the LMC, offer interesting dynamical information that we examine in greater detail in figures 4 and 5. In the lower panel of Figure 4, in the range of PA’s between 270° and 300° , the H I samples of greatest density are seen

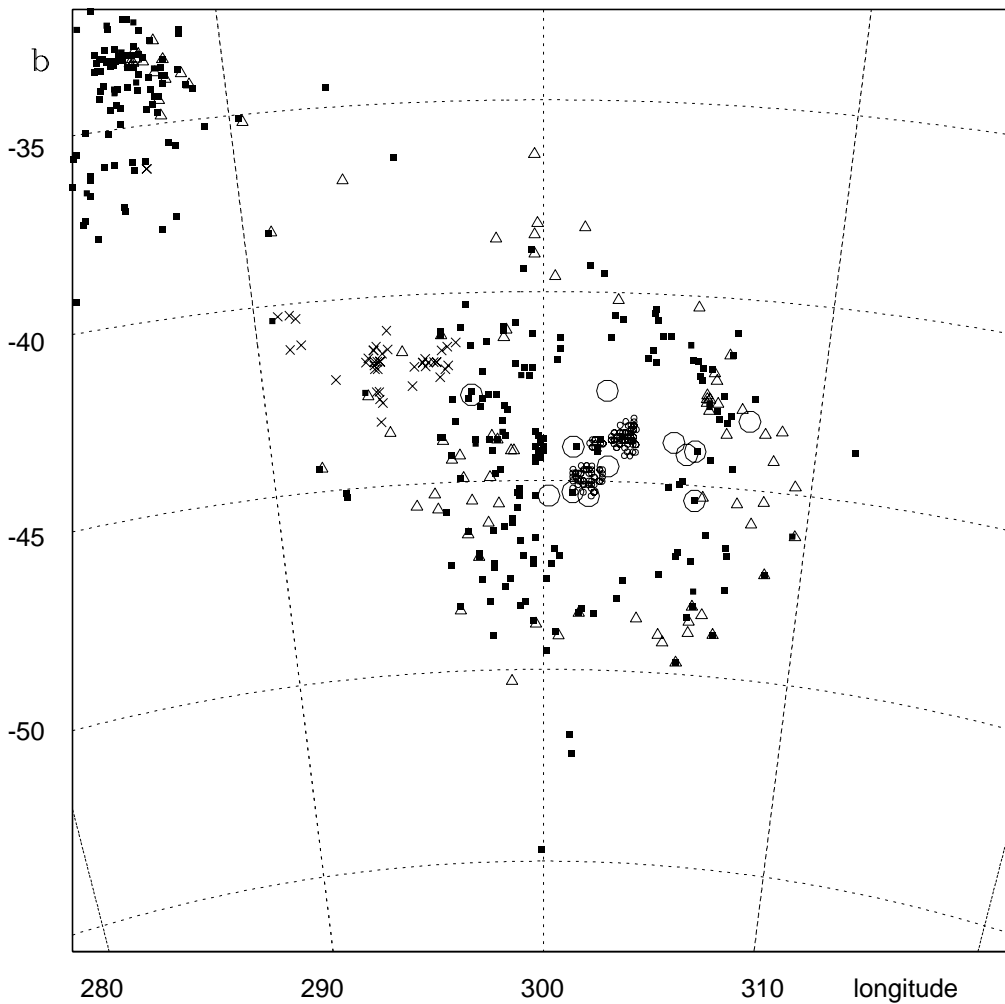


Fig. 2.— A projection on the sky of the carbon stars observed for this investigation (filled squares), the carbon stars observed by Hatzidimitriou *et al.* (1997) (open triangles), the carbon stars of Hardy, Suntzeff & Azzopardi (1989) (small open dots “caviar”). Star symbols are stars of early spectral type. Globular clusters are shown as large open circles.

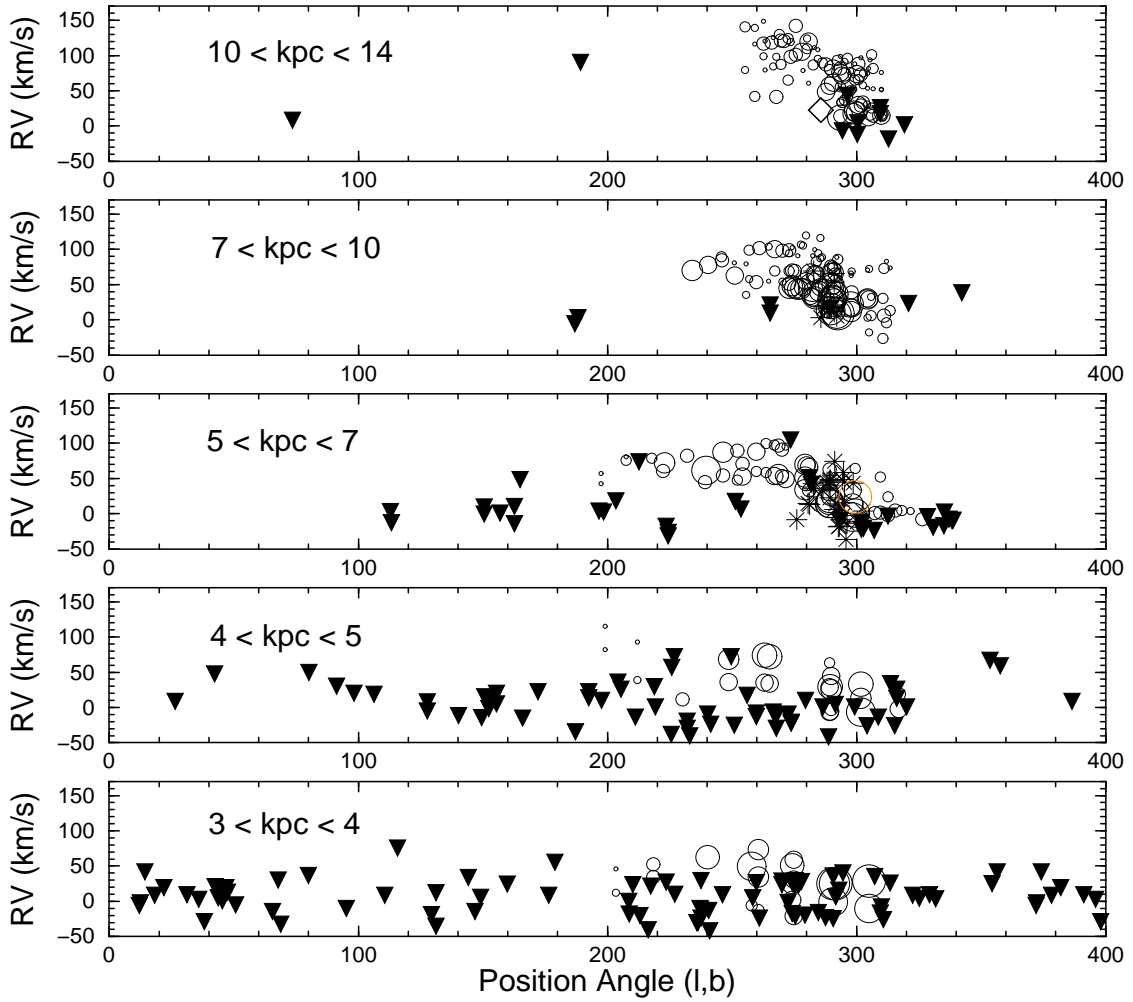


Fig. 3.— Radial velocity of carbon stars (filled triangles), early type stars (stars), and samples of HI (open circles) from McGee & Newton (1986) are shown as a function of position angle about the SMC photocenter (ref) in 5 annular zones, from bottom upward, between 3, 4, 5, 7, 10, and 14 degrees, and as many kpc at the adopted SMC distance.

to lie along a spine whose velocity decreases from about $+70 \text{ km s}^{-1}$ at $\text{PA} = 270^\circ$ to 0 km s^{-1} at $\text{PA} = 300^\circ$. The upper panel of the figure shows much the same negative slope, though a bit steeper, from $+100 \text{ km s}^{-1}$ at $\text{PA} = 270^\circ$ to $+15 \text{ km s}^{-1}$ at $\text{PA} = 300^\circ$. The upper envelope of the HI likewise conforms to a similar slope, and, though there are too few carbon stars to convince by themselves, what positive velocity carbon stars appear in the lower panel follow the same trend.

An estimate for the inclination of the SMC orbital plane to the line of sight may be constructed from this gradient in the H I spine and the gradient of the observed radial velocities of the red horizontal branch clump stars in the line of sight, using the data from the eastern edge of the SMC bar (Hatzidimitriou, Cannon & Hawkins 1993). Their velocity gradient of 70 km s^{-1} over a 10 kpc range of distance in the line of sight provides scaling via a transformation between velocity and distance. The energy of motion in the line of sight certainly precludes the continuation of the SMC as a single self-gravitating entity. Hence we adopt an approximate scaling between radial velocity and distance. In the absence of significant rotation in the SMC, and assuming that ICR particles conserve their angular momentum about the LMC/SMC barycenter, two H I samples in the lower panel of Figure 4 separated by 70 km s^{-1} place the more positive sample some 10 kpc more distant. This difference in velocity is seen between the densest samples at $\text{PA} = 270^\circ$ and similarly the densest samples at $\text{PA} = 300^\circ$, whose separation in the plane of the sky is about 3 kpc. Consequently the line of sight lies at an inclination of about $\arctan(3/10) = 17^\circ$ at most. Comparison of the data with simulations described in section 5 suggests that the angle is somewhat less than this.

When comparing the carbon stars in the ICR to the neutral hydrogen data of McGee & Newton (1986), the distribution of the carbons in the ICR is seen at generally more negative velocities for any position angle or distance from the SMC, almost forming the low velocity envelope, as is apparent in both panels of Figure 4. Moreover, the most positive velocities are found to just one side of the direction toward the LMC: the northern ($\text{PA} < 295^\circ$). The positive velocity domain is not devoid of carbon stars. Two are shown to lie at the upper envelope of the H I. Figure 5 demonstrates the effect in a pair of “fan” plots sampling two triangular areas spaced symmetrically about the direction toward the LMC. The fans show radial velocities of particles lying within a narrow range of position angles seen from the SMC photocenter, as a function of radial distance from the SMC photocenter toward the LMC. The North fan ($250^\circ < \text{PA} < 290^\circ$) is dominated by neutral gas (open circles with diameters corresponding monotonically to H I surface density), containing but three carbon stars in the range between 7 and 14 kpc, while in the same distance range the South fan ($300^\circ < \text{PA} < 340^\circ$) contains 7 carbon stars. Interestingly, the radial velocities of the carbon stars in both fans lie within or at the lower velocity envelope defined by the gas. Other traits distinguishing the two fans are (1) the comparative dearth of neutral hydrogen in the South fan, and (2) the pronounced dense clump of carbon stars in the South fan in the radial range $14.8 < \text{kpc} < 16.9$ only weakly seen in the North fan.

Several interpretations are implied by these observations. First, with the position of the SMC behind the LMC (and hence behind the LMC/SMC barycenter) orbital motion places the South

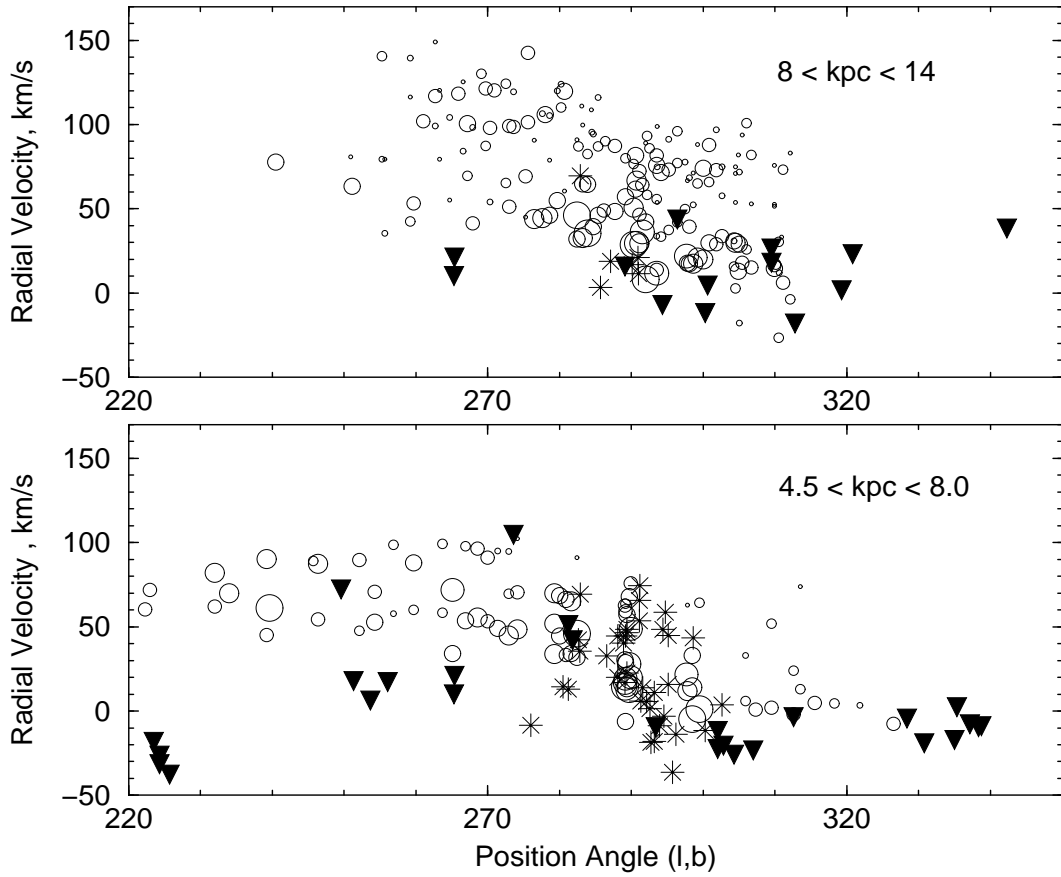


Fig. 4.— Panoramic view of radial velocities in two annular zones, toward the direction of the LMC (PA = 295°) of carbon stars (filled triangles), early type stars (stars), and samples of H I (open circles) as seen from the SMC photocenter.

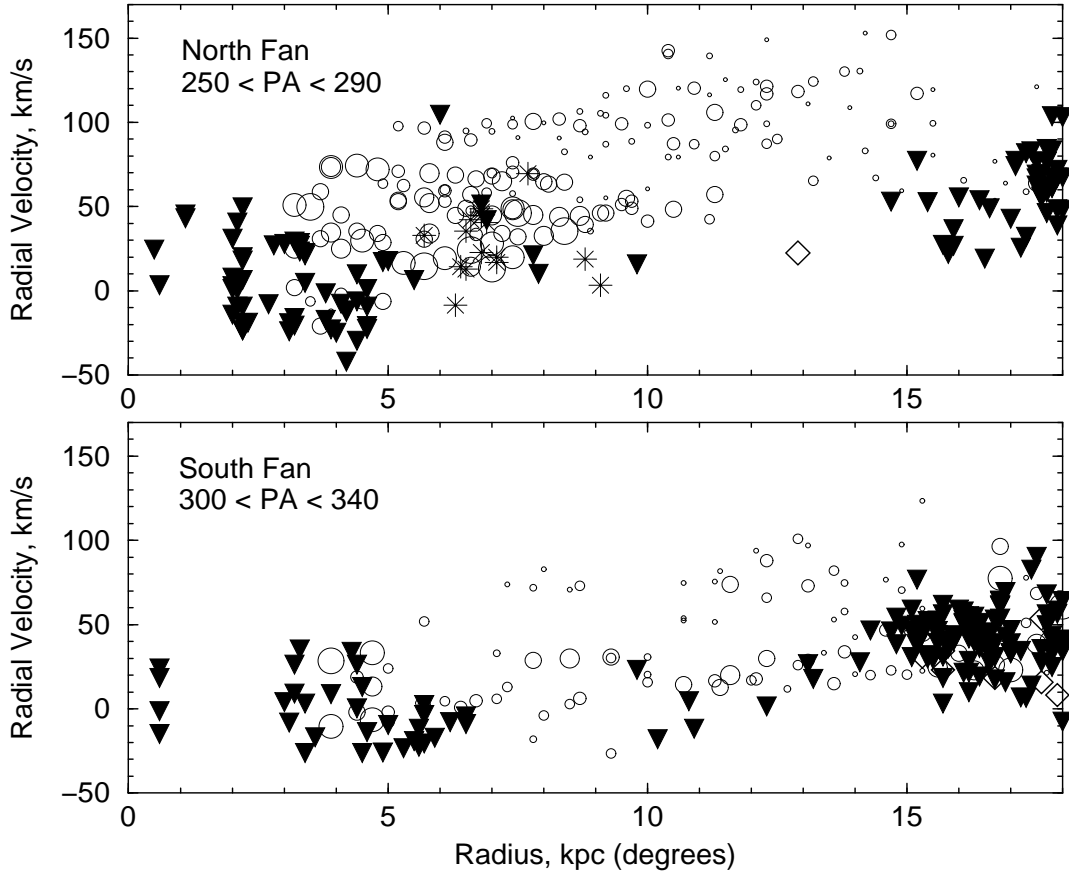


Fig. 5.— “Fan” plots showing radial velocities of particles (symbols as in figure 4) as a function of radial distance from the SMC photocenter. The upper panel includes particles lying at PA’s between 5 and 45 northward of the direction to the LMC, and the lower panel shows particles in the fan between 5 and 45 degrees south of the direction toward the LMC.

fan closer to the observer, and similarly, places the bulk of the gas at distances greater than the ICR carbon stars. Furthermore, though less obvious, we note that in those portions of the diagrams where there is a separation between carbon stars and gas, that separation is consistently less when comparison is with the more massive (denser) H I samples. It is as though the mechanism segregating the carbon stars from the gas were tuned to density, affecting the denser H I clouds in the same way. It is worth re-stating this finding in a converse sense: that the particles most affected by the separating mechanism are the H I samples of lowest density. Last, we attach importance to the fact that whatever mechanism has depleted gas from the forward edge of the orbiting SMC gas, even the most remotely trailing gas is not totally devoid of stars, as the two carbon stars in the lower panel of figure 4, at $(RV, PA) = (71 \text{ km s}^{-1}, 249^\circ)$ and $(106 \text{ km s}^{-1}, 273^\circ)$ demonstrate. The interpretation of these features of the data is delayed to section 6.

Stars of early spectral type are seen superposed preferentially on the denser agglomerations of H I, with a slight preference for the more negative velocities. In all, the inhomogeneous distribution of the debris material suggests that the side nearest the observer, the low velocity edge, has experienced a significant depletion of the neutral hydrogen, since otherwise, with gravity alone acting, the ratio of carbon stars to gas should not vary with velocity as is seen to prevail over most of the ICR.

In closing this section we note that our interpretation of the sense of orbital motion poses no conflict with the orientation of the SMC bar reported by Mathewson, Ford, & Visvanathan (1986, 1988) and Hatzidimitriou & Hawkins (1989) and Hatzidimitriou, Cannon, & Hawkins (1993) which places the NE end of the bar closer to us. This apparent discrepancy merely indicates that the SMC bar does not move parallel to its orientation in space, but “yaws” southward, much as the orientation of an aircraft is seen to “yaw” with respect to its flight direction in a crosswind.

5. INTERPRETATION

The search for an interpretive paradigm relies on dynamical simulation using a simple n-particle “PP code” in which the LMC and SMC are represented by approximately 1500 particles each, allowing them to adjust their potentials under self-gravitation. The purpose of such a simulation is to guide the search for orbital and structural parameters describing each of the Clouds and the details of their interaction, in which discrepancies between a simulation and observations can serve to (1) seek improvements in the simulation, (2) guide the observational program during its development, and (3) steer the interpretation effort around unsuspected pitfalls, of which the most problematic is that of learning what happened to the primordial internal angular momentum (spin) of the pre-encounter SMC disk. The second aspect controlled the last two years of the observing program and the first two have by now been met.

5.1. *The paradigm*

A search for a compact description of the interaction between the Magellanic Clouds will not be advanced significantly if the simulation is required to model every and all physical processes one observes or might consider interesting, including for example the star formation precipitated by a tidal impulse, and which we see unevenly distributed over the face of the SMC. The approach preferred here seeks to *minimize* the number of parameters needed to describe the essentials of the gravitational interaction alone between particles that experience no internal evolution during the time interval studied, and to exclude other forces, such as those arising through hydrodynamics or from magnetic fields. Some detail important to local astronomical processes will be lost, such as the distribution of star formation regions or the energy input to the ISM from supernova events. We call this approach a minimum parameter technique (MPT). Its principal aims are (1) to test the adequacy of interpreting a tidal disruption as dominated by gravity alone on visible particles only, and (2) to indicate something of the character of additional physical mechanisms (or particles) that may affect the kinematics observed.

The motivation for preferring the minimization of the parameter count is not merely philosophical but is rooted in the nature of the mathematical character of our search. In practice, even at the outset, a large proportion of the parameters controlling a simulation can be narrowly constrained, such as the coordinates of the major perturbers in phase space. If all but a very few parameters can be specified in advance, the simulation should rapidly achieve its goals. However, as the count k_f of free parameters increases, the volume of neighboring parameter space that must be searched at each integration step rises explosively, the effort to search the neighboring pieces of parameter space increasing roughly as 2^{k_f} at each occasion. Such a search cannot be expected to converge speedily to the description sought, however. In a worst case 2^{k_f} simulations are required before a succeeding iterative step in parameter space may be chosen optimally. And worse still, there is nothing but faith to sustain the belief that the topology of the immediate neighborhood in this parameter space is well behaved (continuous and differentiable), so that iterative methods stand a chance of converging. Our experience has shown that at least one parameter is formally chaotic: disk structures are affected by the Toomre instability to bar formation. Moreover, our methodological simplification introduces other difficulties in choosing the next time step. In advancing a simulation step truncation errors sum, and the graininess inherent in the small count of particles requires control, and we have followed the guidelines recommended by Merritt (1996). For example, a minimum particle count was determined running simulations with different particle counts and observing the precision with which descriptive detail settled to a unique configuration at some minimum value; runs with at least double, and usually five times such minimum values were used to constrain the buildup of error. In effect, beyond the summing of errors, the topology of parameter space has become fractal. In practical terms, the significance is that there is no assurance that iterative methods can explore the entire parameter space one would like to dominate. Simple iterative strategies can explore only a small fraction of parameter space, and this limitation forces us to adopt a compromise: By minimizing the count of parameters some cosmetic detail in

the simulation may appear deficient in describing the observations. However, the investigator may decide later, after a number of iterative improvements have been achieved, if the acceptance of such concessions has derailed the exercise. It is the fractal character of parameter space that leads to the following caveat: just because a simulation has been found that matches an aspect of the observations for some interesting combination of parameter values one has no assurance that the neighborhood of the solution judged as acceptable is multiple or single valued, and whether other, physically more meaningful parameter combinations may lie nearby. Historical examples of such circumstances now merit review, and a few will be briefly mentioned further on. An anonymous precaution summarizes this dilemma and is worth keeping in mind: “all simulations are doomed to succeed!” (Welch, 1998), and increasing the parameter count beyond an MPT aggravates this situation.

5.2. Parameter choices

The simulation shall describe the interaction of the Magellanic Clouds in their motion about the Milky Way. More remote perturbers, such as M31, are not treated: as without significance during the 1.2 Gyr duration of the simulations. There are 26 parameters that are deemed to constitute a minimal configuration. Their initial values (count in parentheses), and their search ranges are:

1. The mass ratios (2; 1 free)

- (a) $\mathcal{M}_{SMC}/\mathcal{M}_{LMC} = 0.25$

- (b) $0.007 < \mathcal{M}_{SMC+LMC}/\mathcal{M}_{Galaxy} < 0.05$

2. Phase space (12; 1 free)

- (a) Positional coordinates are adopted, setting radial distances as 50 and 58 kpc for the LMC and SMC, respectively.

- (b) For both Clouds the velocity in the line of sight is adopted from the observations. For both Clouds the direction of motion in the plane of the sky is taken to be that of the Magellanic Stream.

- (c) The speed of the LMC can be solved for by the method of Feitzinger *et al.* (1977): we adopt that transverse speed for which the line of nodes retains the least warping ($= 240 \text{ km s}^{-1}$), which is close to the 215 km s^{-1} obtained by Jones, Klemola and Lin (1994) for an LMC mass closest to our earlier value (Paper III). For the SMC we adopt a transverse speed 60 km s^{-1} less, in conformity to the geometric and timing constraints (since pericentric passage).

- (d) The motion of the SMC perpendicular to the Magellanic Stream is constrained by the inclination of the SMC orbit to the plane of the sky (section 4 above).

3. Spin orientation (6; 2 free)

- (a) The spin of the of the Milky Way is relatively unimportant for the simulation. Motion of the LSR was set to 225 km s^{-1} .
- (b) An inclination of 33° and line of nodes for the LMC is adopted from Feitzinger et al. (1977).
- (c) There is no indication in the observations of the SMC that any meaningful tracer of spin information is preserved; in comparison to other motions the enormous extent of the SMC in the line of sight suggests that there may no longer be any significant spin. In many ways this is the most demanding constraint on the simulation, and especially for a description of the SMC core.

4. Structure (6; 3 free)

- (a) The question of the number of parameters describing the disk and/or halo structure is the most debated among aficionados of simulations. In conformity with the MPT approach a minimum choice must include a scale length, a scale height, and the fraction of the total energy of internal motion that shall be contained in particle heat (instead of cold rotation). The last two quantities are not independent. Stability of the disk against bar formation is controlled by Toomre’s Q . No halo component as a separate entity is provided; its separate inclusion would augment the parameter count by six, requiring too much arbitrariness in devising an iteration strategy. Furthermore, since tidal action must affect dark and luminous matter similarly, we cannot find [devise] a rationale for treating their dynamics separately.
- (b) We adopt an LMC scale length of 1.7 kpc (Feitzinger 1980). We adopt (arbitrarily) an axis ratio (scale height) of 0.3, and a velocity dispersion (heating) to bring the quiescent disk to the point of bar instability. The resulting particle dispersion in the simulation amounted to 19 km s^{-1} , not far from the 16 km s^{-1} observed in the LMC carbon stars (Kunkel *et al.* 1997).
- (c) There is no indication about what structure the SMC may have had prior to its encounter with the LMC. A relatively cool disk similar to that adopted for the LMC appears unlikely; in the absence of a pre-encounter SMC bar all simulations show that following an interaction a significant portion of internal spin should have been preserved, and no evidence for such spin is found in any observations of the SMC bar. Far greater disruptive damage to the SMC periphery would be required than that observed to mask

the residual spin. In view of the fractal character of parameter space, we consider that several choices of a pre-encounter configuration produce equally valid SMC Wing structures. The structures so far explored are either an essentially spin-free spheroidal configuration reminiscent of the dSph systems, or, what seems more likely in view of the high incidence of internal bars Odehahn (1994) finds in Magellanic satellites, a strongly bar-like system with the bar orientation at pericentric passage along a line of strongest tidal shear.

5.3. *Summary of the simulations*

Of the 26 parameters selected, 7 are considered “free”, in that they are allowed to vary over a reasonable range, permitting some adjustment of the match between the simulation and the observational data. Some parameters appear quite “robust”, varying independently of the others. Most noteworthy in this sense is the total Magellanic Clouds-to-Galaxy mass ratio, $\mathcal{M}_{SMC+LMC}/\mathcal{M}_{Galaxy}$. Within the tested range the value of this quantity was found narrowly constrained to lie between 0.020 and 0.030, and will be more carefully discussed in a later paper dealing with the carbon stars of the Large Magellanic Cloud.

The free phase space parameter (of 12) is the proper motion of the SMC southward with respect to the SMC,LMC pericenter. The rationale confining this quantity was explored in section 4.0 above, and is basically determined by the discussion surrounding Figures 3 and 4.

The two parameters governing the spin orientation and the three disk structural parameters were the outstanding headache dominating the selection of simulation parameters. The principal difficulty consists in the fact that any significant spin in the pre-encounter SMC disk, if present, survives the encounter to excessive degree for all reasonable orbital impact parameters at the current SMC/LMC encounter. Adding a “massive dark matter halo” on a scale other than “mass follows light” to the SMC or LMC acts in the wrong sense, aggravating the dilemma. In fact, the most satisfactory “fits” to the observed distribution of SMC material were obtained by leaving the pre-encounter SMC virtually devoid of any pre-encounter spin at all! The most influential parameter affecting the “goodness of fit” was found to be the Toomre Q, and for the small particle count in our simulation that parameter behaves formally in a chaotic manner. In practical terms, we found that when the Toomre Q was set close to its critical value, even an infinitesimal variation in some other parameter affecting the SMC/LMC encounter (such as a small change in the particle count!) elicited major variations in the resulting debris distribution. Our primary conclusion regarding the remaining five “free” parameters is that, were one to assume a typical disk structure as observed in other dwarf disk systems of comparable luminosity, then our simulations were unable to find a configuration with a spin amplitude typical of what one associates with a dwarf galaxy of the SMC’s luminosity. Alternatively, were the pre-encounter SMC endowed with a significant bar, then the orientation of that bar during the encounter often dominates the later debris distribution. Even then, however, any “reasonable” spin attributed to the SMC spreads debris over too wide a swath

between the Clouds, unless one reduces the SMC/LMC mass-ratio, as was done by Fujimoto & Sofue (1976, 1977), Murai & Fujimoto (1980) and in the later simulations of Gardiner & Noguchi (1996). In summary: a good fit to the SMC Bar and Wing can be attained for a varied choice of structural parameters, most easily by keeping the SMC’s spin low and “leaning” the pre-encounter bar to the “right” angle. The vagaries of the Toomre Q limit the effectiveness of such a search, and finding one satisfying configuration does not signify that others, with equally valid parameter values, may not exist. We believe the solution to this problem to be multi-valued, so that without additional observational data any one successful simulation tells little of what actually happened.

The bottom line of this inquiry may well be that one must treat the role of massive dark matter haloes with care if the absence of SMC core spin is to be adequately represented.

6. CORROBORATING DATA IN THE LINE OF SIGHT

A demonstration that tidal disruption has affected the SMC throughout its entire volume may be appreciated from component population inhomogeneities in the line of sight (LOS) toward the photocenter of the SMC where no visible effects appear in direct imaging. This demonstration depends on the reasoning employed to determine the SMC’s orbital inclination in section 4 above. If we accept that the SMC is currently experiencing a breakup in the LOS direction, as has been suggested by the distribution of Cepheid variables studied by Mathewson, Ford & Visvanathan (1986, 1988), and more clearly in Red Horizontal Branch stars on the eastern edge of the SMC bar (Hatzidimitriou & Hawkins 1989, Hatzidimitriou, Cannon, & Hawkins 1993), then it becomes reasonable to ask whether, during such a breakup of the SMC, the radial velocity of any SMC object also reflects, at least in part, the position of such an object in the line of sight. More specifically, for such objects known to show low velocity dispersions in the LMC, Hatzidimitriou (1998) finds significantly the higher velocity dispersions in the SMC among all classes of SMC objects investigated, pointing to the presence of an expansion component that all share uniformly.

This circumstance provides an unusual opportunity to conduct a simple observational test that is entirely independent of any physical or dynamical model, and in particular, one which avoids all dependence on reddening that normally plagues investigations of distributions in radial distance. In this test, radial velocity is proposed as an indicator of relative distance, with a scaling adopted from Hatzidimitriou et al (1993) of 7km s^{-1} per kpc. The validity of such relative scaling rests on the conservation of angular momentum of the SMC fragments about the SMC/LMC barycenter. Such a test will prove more sensitive for objects known to show the lower velocity dispersion, such as H I, stars of early spectral type, cepheids, supergiants, and, yes, carbon stars, given their low intrinsic velocity dispersion observed in the LMC (Kunkel *et al.* 1997). In the application proposed here, the test is formulated as a null hypothesis which predicts the following: Under gravity acting alone, if no disruptive expansion were taking place, then in the absence of inhomogeneity the median radial velocity observed for all classes of objects should be the same. Further, half the objects of any class should lie in front of, and half behind this median velocity. Moreover, if the

velocity dispersion for two classes of objects that are compared is the same, or small compared to an expansion, distribution curves for both classes run parallel. This last concept can be stated more conveniently: the ratio of the portion of one class lying in front of any point scaled in that class along the line of sight should be the same as for the other class, irrespective of distance. So, for example, an object of the first class, lying behind, say, eighty percent of its own class should lie behind eighty percent of the other class as well.

A visual demonstration is most readily arranged in some convenient sequential counting order, using as independent variable the gas fraction (of H I) with a velocity less than that of the carbon star (i.e., the gas fraction lying in front of the star), determined from planimetry under the HI velocity profile. Carbon stars embedded uniformly in the gas should lie on a straight line of unit slope. This choice of independent variable offers several advantages. One is that “self-propagating star formation” and other non-uniformities affecting the distribution of young objects in the gas are circumvented. Another is to test the relation between the SMC and the Magellanic Stream: If, following current lore, the Magellanic Stream is devoid of stars, then the cumulative distribution of carbon stars should form a straight line broken on the near low side if the Stream lies in front of the SMC, or at the high end of the data set if it lies behind the SMC. In either circumstance, with the presence of the Stream a slope greater than 1.0 is expected everywhere except at the Stream, where a much flatter, or zero slope should prevail. Again, if velocity dispersions of the gas and stars are very dissimilar, so that stars have traveled further in the line of sight than the gas, a flat curve is expected, with very steep slopes $\gg 1.0$ at both ends, symmetric about the median velocity of the gas. Last, if no breakup is occurring, and velocity is no indicator of distance in the line of sight, then perfect mixing should prevail; which is to say that a slope of unity is expected over the entire range of the distribution. On the other hand, if radial velocity does reflect relative distance, a slope less than 1.0 over a significant portion of the distribution signifies a prevalence of H I over the affected portion of the corresponding distance scale, and that any explanatory dynamics cannot be attributed to gravitational forces alone.

A cumulative distribution of the carbon stars from Hardy et al (1989) as a fraction of the gas (Mathewson *et al.* 1988) is shown in Figures 6. The power of this test is predicated on the age of the carbon stars, which is greater than the time elapsed since the LMC/SMC interaction. Since the stars are older, gravitational forces mediating the tidal effects alone act on them, and deviations from the distribution of the carbon stars necessarily reflect additional dynamic processes operating on the gas. The null hypothesis (absence of additional gas processes) requires a straight line of unit slope, and it is apparent that for neither the SW bar of the SMC (lower panel of Figure 6), nor the NE bar (upper panel) can this condition be said to hold. Even in the more uniform sample (the SW panel), drawn from within one degree of the photocenter of the SMC, one perceives two slopes, with a break at a point two thirds from the front of the SMC. Compared to the front two thirds of the mass distribution mapped by the carbon stars along the line of sight, for which the ratio of gas-to-carbon-stars remains constant, the back third is quite unevenly mixed, with nearly a factor of two excess of gas between $F = 0.64$ and $F = 0.84$, and almost no H I at all for the last 15 percent

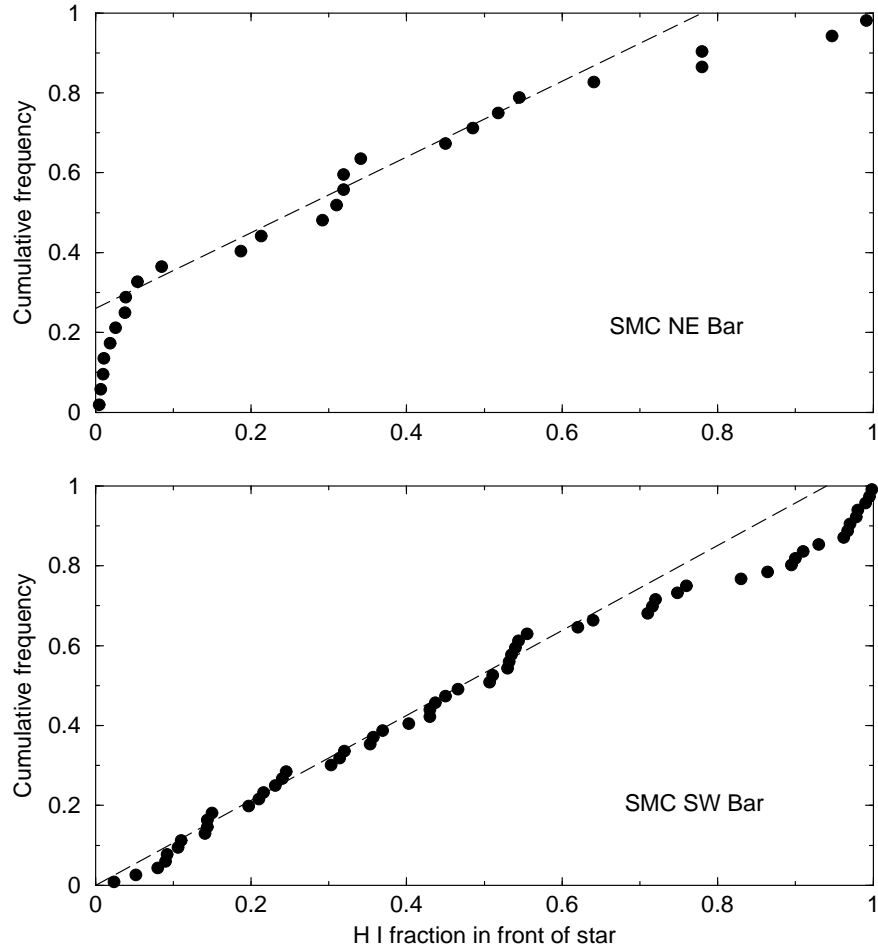


Fig. 6.— Cumulative distribution of carbon stars (from Hardy, Suntzeff, & Azzopardi 1989) as a function of the hydrogen fraction (from Mathewson *et al.* 1986) lying in front of a star. The Southwest Bar is shown in the lower panel, and the Northeast Bar is shown in the upper panel.

of the carbon stars. The situation in the NE bar is more extreme, with the front third of carbon stars embedded in less than 5 percent of the H I, and with 70 percent of the H I lying behind the midpoint of the carbon star mass distribution. The interpretation of these data, taken within one degree of the photocenter of the SMC, is that if we are confronted by a break-up of the SMC, then the presence of non-gravitational forces modifying the structure of the gaseous component of this stellar system must act, or other processes ionizing portions of the gas “out of sight.”

The obvious test for the significance of these data is a Kolmogorov-Smirnov ($K-S$) test (Kendall & Stuart 1961). By this test the probability that the observed distribution arises from the same distribution is 11 and 3 percent for the SW and NE sample, respectively. A description of this test by Kendall & Stuart points out that the $K-S$ deviation is taken irrespective of sign, and irrespective of location of the deviation on the abscissa, thereby weakening the discriminative information in the data. By allowing one to select the location of the independent variable, a Monte-Carlo simulation of the null hypothesis places far more stringent limits. In one million simulations less than 1.6 percent deviate more than the SW sample in the lower panel of Figure 6 at $F = 0.88$, and less than 0.03 percent deviate more than the NE sample in upper panel at $F = 0.30$. We note furthermore that in the two fields, the deviation from a straight line occurs at opposite ends of the line of sight. In the SW field the deviation occurs at the far end, with a greater density of carbon stars compared to HI on the nearer side. That is, the gas to stars ratio is greater at the far end of the SMC. Within one degree, in the NE field, a dramatically more pronounced excess of stars occurs at the front end of the SMC, with 30 percent of the stars lying in front of 95 percent of the H I! Our conclusion is that the null hypothesis is rejected with a confidence exceeding 99.9 percent, and forces other than gravity alone are required to explain the kinematics of the SMC.

In terms of dynamical processes the relation of the carbon stars to H I gas is fundamental, and a comparison to young, recently formed populations introduces additional uncertainties associated with the idiosyncracies of star formation during a transient tidal impulse. Still, (and following the referee’s recommendation) there is some interest in comparing the distribution with young populations that in time formed after the tidal impulse. Figure 7 provides this comparison, showing the cumulative distribution of cepheids (from Mathewson *et al.* 1988) and supergiants (from Maurice *et al.* 1989). The upper panels show the cumulative distribution in terms of heliocentric radial velocity for the carbon stars, by a continuous line, which differs from that of stars formed after the tidal impulse: the cepheids and supergiants, indicated by open circles and filled diamonds, respectively. While the asymmetric distribution in the NE bar may result from a unique process, that seen in the SW bar represents a puzzle which is not resolved by postulating significantly different velocity dispersions for the three populations compared. It is worth noting that a dynamical explanation for the observed discrepancies, based on differences in intrinsic velocity dispersions, should be symmetric about the centers of the plots, at $F = 0.5$, and such symmetry is nowhere in evidence. The young populations of the NE bar, lying at more positive velocities at all positions in the line of sight, appear to occupy the rear of the stellar volume mapped by the carbons stars (lower panel). In the SW bar no comparably simple explanation for the onset of the distribution discrepancy at

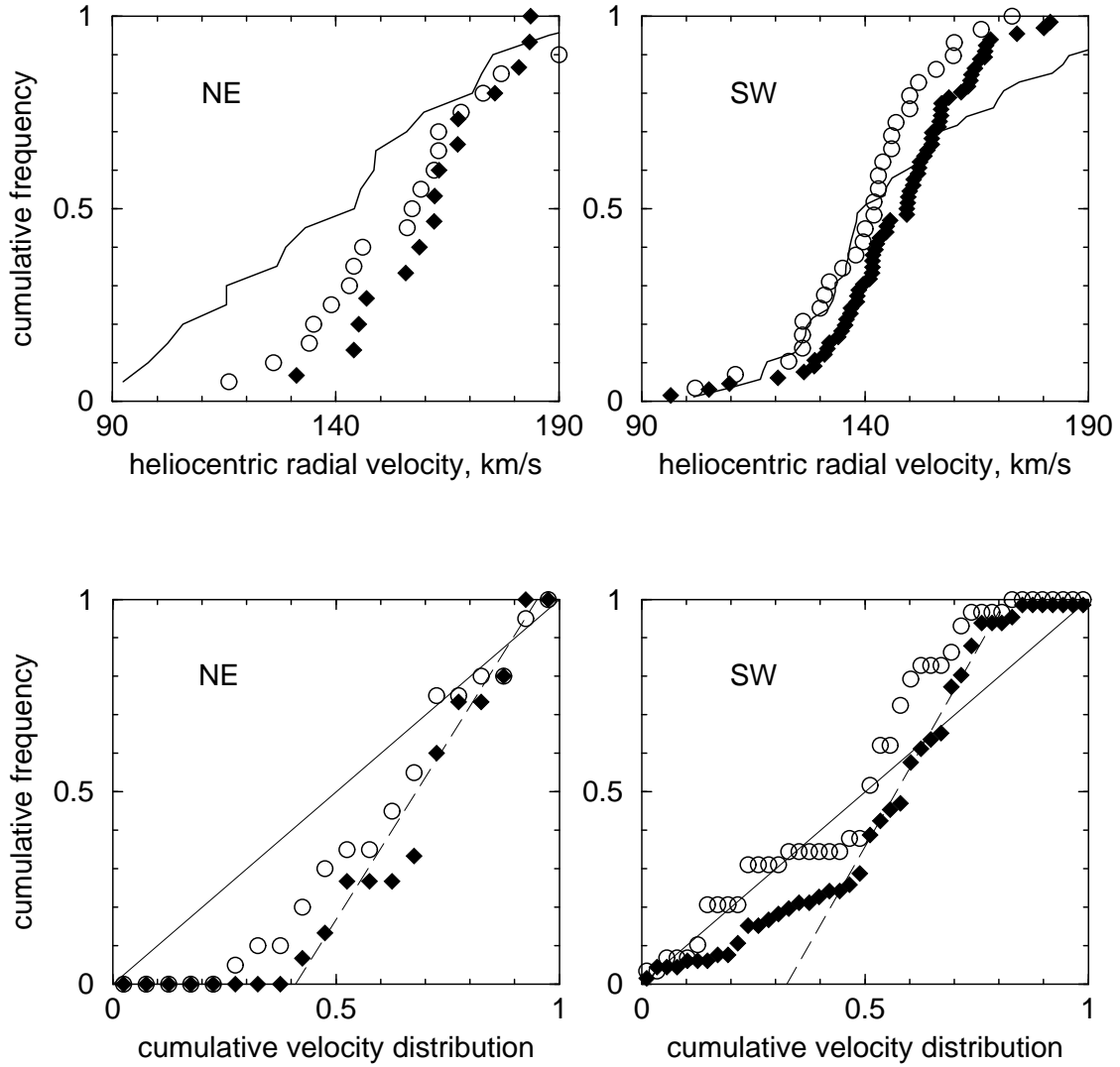


Fig. 7.— Cumulative distributions of cepheids (open circles), supergiants (filled diamonds), and carbon stars (continuous line) toward the NE and SW of the SMC bar as a function of the heliocentric radial velocity (upper panels) and the carbon star mass distribution (lower panels). See text.

velocities more positive than 140 km s^{-1} suggests itself.

7. SUMMARY AND CONCLUDING REMARKS

The kinematics of 150 carbon stars on the periphery of the Small Magellanic Cloud shows an asymmetric distribution characterized by a total absence of rotation at radii between 3 and 8 kpc.

Beyond 5 kpc the distribution of the carbon stars becomes increasingly asymmetric, with a marked deficiency in the quadrant centered to the South of the SMC. At radii beyond 7 kpc the carbon stars cluster on the position angle in the direction toward the LMC $PA(l,b)=295^\circ$. In the region between 10 and 14 kpc the 7 carbon stars found all lie in a 15° sector immediately to the South of this same direction, leaving the quadrant to the North vacant.

With but two exceptions the velocities of the carbon stars found beyond 5kpc from the SMC photocenter are seen at the low velocity envelope of the neutral hydrogen mapped by McGee & Newton (1986). Further, we note that the H I elements of higher density as well as most of the early type stars lie at this low velocity envelope.

The distribution of material in the ICR is asymmetric about the direction toward the LMC in other respects. Beyond 5 kpc the northern “fan” (Figure 5, upper panel) contains most of the HI and relatively few ICR carbon stars, while the southern fan (Figure 5, lower panel) contains most of the ICR carbon stars, and less than a quarter of the ICR H I.

In the direction toward the LMC the kinematic asymmetry of material in position angle is most apparent for $PA(l,b)$ between 270° and 300° . In this range the slope of the spine of densest H I elements is negative, from 70 km s^{-1} at $PA = 270^\circ$ to 0 km s^{-1} at $PA = 300^\circ$. From this we infer an inclination of the SMC’s orbit about the LMC/SMC barycenter of 73° to the plane of the sky.

While the asymmetries at radii beyond 5 kpc from the photocenter arise from a comparison of carbon star kinematics with those of H I and early type stars, a corresponding asymmetry is seen in lines of sight toward the photocenter, in an inhomogeneous distribution of the carbon stars observed by Hardy, Suntzeff, & Azzopardi (1989) when scaled to the H I distribution mapped by Mathewson, Ford, & Visvanathan (1988). A deficiency of H I is seen on the near side, and a comparative excess of H I on the far side. This inhomogeneity is found incompatible with an homogeneous admixture at a level of 0.03 percent.

The conclusion becomes inescapable that in addition to gravity other forces act that significantly modify the motion of the gas throughout the entire SMC. One is tempted to consider these phenomena in the same context first examined by Moore & Davis (1994), who proposed two mechanisms capable of generating a separation akin to that found here. One is the action of a collision impulse at pericenter during the LMC/SMC encounter that incrementally decreased the orbital momentum of the SMC gas interacting with the LMC disk gas. That interaction should not affect the SMC stars. The alternative mechanism is the continuous action of ram pressure during the

motion of the SMC through the local hot Galactic corona. The three body character of the problem defeats intuitive insights into deciding which of the two proposed processes dominates. While we may not yet be able to decide the manner in which these two mechanisms combine, it seems worth noting that, whatever the combination, in the end most of the gas of the recent LMC/SMC interaction is found preferentially in the tidal tail (while stars dominate in the bridge). Thus, although both the tail and the bridge lie projected on the sky in the ICR, the formation events appear to be of the same form as whatever process formed the Magellanic Stream proper, and may not require the special binary relation between the LMC and SMC postulated as essential so as to deposit debris into the “tail alone” as proposed by Murai & Fujimoto (1980).

Instead, we are reminded, rather, of the syndrome experienced by UGC7636 after its interaction with NGC4472 (Sancisi, Thonnard, & Ekers 1987, and Patterson & Thuan 1993). Here the photographic appearance of UGC7636 shows faint evidence of a tail, *without* a leading bridge (Arp 1966). The detailed VLA H I map of McNamara *et al.* (1994) shows the H I of UGC7636 confined entirely to the tail alone, and photometry of several star clusters that formed in the tail gas after the interaction (Lee, Kim, & Geisler 1997). Of course, the density of the hot gas envelope centered on NGC4472 provoking the syndrome seen in UGC7636 is some 20 times greater than that inferred for the Magellanic Stream (Weiner & Williams 1996, and Sancisi, Thonnard, & Ekers 1987), and so, quite unsurprisingly, the phenomenology seen in the SMC is correspondingly milder.

Nonetheless it seems appropriate to end with a cautionary note that when we talk of the haloes of dwarf galaxies we refer to dynamically stationary settings, where things remain structurally well ordered. Here our description of the SMC is of a setting in which recent dynamical violence has disrupted whatever order may once have existed. In such circumstances to talk about a halo is likely to mislead our thinking.

This project is supported financially, in part (S.D.) by the Natural Sciences and Engineering Research Council of Canada.

A. Appendicial material

Star names are based on the field in which they are found, followed by a number corresponding to our candidate list. Subsequent columns give: equatorial coordinates; the averaged heliocentric radial velocity; the radial velocity corrected for solar motion $U, V, W = 9, 12, 7 \text{ km s}^{-1}$, adopting $V_{\odot} = 225 \text{ km s}^{-1}$; the spectrum quality parameter Q (see Kunkel, Demers, & Irwin (1997) for an explanation); the number of spectra obtained; a magnitude; a color; and remarks when appropriate.

Table 1. Small Magellanic Cloud periphery carbon stars

Name	id field	RA (1950)	Dec	ℓ	b	v_{helio}	v_{gc}	Q	n	R	$B_j - R$	comments
C0142-7219	029-010	1 42 03.7	-72 19 48	318.1	-39.8	122.0	-9.2	7	1	15.4	3.45	
C0136-7239	029-023	1 36 16.6	-72 39 55	298.1	-44.2	173.3	15.5	7	2	16.0	3.17	
C0141-7243	029-031	1 41 51.3	-72 43 52	297.5	-44.0	144.4	-14.6	7	1	15.6	2.53	
C0142-7251	029-035	1 42 48.4	-72 51 48	297.5	-43.9	128.9	-30.4	7	2	15.6	4.53	
C0137-7257	029-039	1 37 42.9	-72 57 20	298.0	-43.9	166.6	7.9	7	1	15.6	3.41	
C0134-7301	029-040	1 34 55.7	-73 01 29	298.3	-43.9	174.3	16.0	7	1	15.8	2.90	
C0130-7312	029-048	1 30 32.7	-73 12 55	298.5	-43.7	125.9	-32.6	7	1	15.7	2.94	
C0135-7331	029-066	1 35 11.3	-73 31 33	298.5	-43.4	129.8	-29.4	7	1	15.6	4.10	
C0144-7347	029-098	1 44 04.1	-73 47 18	297.7	-43.0	125.1	-36.1	7	1	15.4	2.82	
C0143-7356	029-110	1 43 59.1	-73 56 03	297.8	-42.8	184.7	23.0	7	1	15.6	2.72	
C0141-7403	029-123	1 41 53.1	-74 03 16	298.0	-42.7	164.6	2.9	7	1	15.9	2.65	
C0134-7505	029-218	1 34 26.4	-75 05 26	299.0	-41.9	131.9	-30.3	7	1	15.6	2.95	
C0118-7521	029-232	1 18 04.6	-75 21 11	300.5	-41.8	150.5	-9.8	7	1	15.6	2.99	
C0117-7539	029-243	1 17 09.5	-75 39 46	300.6	-41.5	156.0	-4.8	7	1	16.3	2.93	
C0149-7525	029-244	1 49 33.3	-75 25 53	298.0	-41.3	137.9	-27.1	7	1	16.8	3.99	
C0020-7527	029-247	0 20 39.6	-75 27 13	305.3	-41.7	140.8	-12.1	7	1	15.0	3.33	
C0130-7554	029-259	1 30 34.5	-75 54 26	299.6	-41.1	158.4	-4.8	7	1	15.3	2.61	
C0142-7549	029-261	1 42 49.9	-75 49 23	298.6	-41.0	125.2	-39.6	7	1	15.8	3.69	
C0118-7559	029-263	1 18 12.4	-75 59 57	300.6	-41.2	150.9	-10.6	7	1	16.4	4.03	
C0057-7603	029-265	0 57 03.5	-76 03 11	306.8	-40.9	184.3	32.2	7	1	16.3	2.57	
C0055-7603	029-267	0 55 59.7	-76 03 14	302.4	-41.2	169.5	10.6	7	1	15.8	2.46	
C0058-7613	029-268	0 58 33.2	-76 13 01	304.2	-41.1	149.9	-6.2	7	1	15.7	4.59	
C0138-7609	029-270	1 38 56.7	-76 09 24	299.0	-40.8	151.6	-13.1	7	1	15.6	2.43	
C0050-7635	029-278	0 50 15.6	-76 35 17	302.8	-40.7	165.8	6.5	7	1	15.6	2.69	
C0055-7644	029-279	0 55 17.5	-76 44 35	302.5	-40.6	187.4	27.4	7	1	16.2	2.44	
C0036-7650	029-282	0 36 30.9	-76 50 03	303.9	-40.4	138.0	-20.1	7	1	15.4	2.68	
C0141-7731	029-289	1 41 04.3	-77 31 55	299.3	-39.4	134.5	-33.0	5	1	15.4	2.61	M
C0102-7749	029-290	1 02 15.2	-77 49 38	302.1	-39.5	216.0	60.5	7	1	15.8	2.72	
C0155-7238	030-02	1 55 21.0	-72 38 13	296.2	-43.8	97.8	-63.3	7	1	15.6	3.83	
C0154-7238	030-03	1 54 11.7	-72 38 53	296.3	-43.8	125.7	-35.3	7	1	14.8	2.80	
C0151-7306	030-09	1 51 02.1	-73 06 54	296.8	-43.4	158.4	-3.0	7	1	14.8	2.88	
C0132-7309	030-11	1 32 23.2	-73 09 30	298.6	-43.8	172.7	14.5	7	1	15.5	3.17	
C0155-7343	030-15	1 55 29.4	-73 43 16	296.7	-42.8	151.2	-11.8	7	1	15.8	3.31	
C0149-7354	030-18	1 49 56.2	-73 54 03	297.3	-42.8	107.1	-37.5	7	1	15.3	2.47	
C0133-7351	030-23	1 33 41.7	-73 51 38	298.7	-43.1	122.1	-37.6	6	1	16.3	2.70	
C0148-7403	030-24	1 48 47.2	-74 03 32	297.4	-42.6	153.6	-9.0	7	1	16.3	3.17	
C0135-7356	030-25	1 35 08.1	-73 56 40	298.6	-43.0	153.6	-6.5	7	1	15.0	2.83	
C0139-7406	030-29	1 39 20.0	-74 06 46	298.3	-42.7	188.4	27.1	4	1	16.9	4.35	wk C
C0147-7437	030-34	1 47 18.4	-74 37 33	297.8	-42.1	151.1	-12.2	7	1	15.1	2.80	
C0131-7447	030-36	1 31 25.2	-74 47 31	299.2	-42.2	183.1	21.8	5	1	14.7	2.58	wk C
C0127-7452	030-37	1 27 49.7	-74 52 03	299.5	-42.2	139.1	-21.6	7	1	14.5	2.94	

Table 1—Continued

Name	id field	RA	(1950)	Dec	ℓ	b	v_{helio}	v_{gc}	Q	n	R	$B_j - R$	comments
C0055-6847	051-15	0 55	32.5	-68 47 54	302.0	-48.5	93.8	-47.7	7	1	15.3	2.76	
C0059-6849	051-16	0 59	53.2	-68 49 23	301.5	-48.4	64.6	-77.9	7	1	15.6	2.54	
C0049-6914	051-24	0 49	21.8	-69 14 29	302.9	-48.1	183.3	41.9	7	1	15.5	3.31	
C0122-6910	051-26	1 22	27.0	-69 10 32	298.5	-47.8	164.7	16.7	7	1	15.2	2.87	
C0047-6942	051-31	0 47	28.5	-69 42 40	303.1	-47.6	137.2	-5.1	7	1	15.4	3.06	
C0036-6954	051-32	0 36	33.0	-69 54 12	304.5	-47.4	151.2	10.3	7	1	15.5	2.56	
C0115-6954	051-33	1 15	43.6	-69 54 30	299.6	-47.2	94.6	-53.5	7	1	15.4	3.55	
C0116-7003	051-35	1 16	00.9	-70 03 25	299.6	-47.1	156.6	8.1	7	1	16.0	2.62	
C0107-7012	051-40	1 07	39.0	-70 12 58	300.6	-47.0	115.7	-31.6	7	1	15.3	2.88	
C0115-7036	051-55	1 15	49.8	-70 36 23	299.7	-46.5	164.2	14.3	7	1	15.5	2.50	
C0124-7105	051-73	1 24	13.6	-71 05 09	298.8	-46.0	168.7	16.3	4	1	15.2	2.83	wk C
C0124-7106	051-76	1 24	52.6	-71 06 11	298.8	-46.0	115.3	-37.0	7	1	15.3	2.42	
C0124-6758	052-04	1 24	26.7	-67 58 33	298.0	-49.1	206.2	61.0	7	1	15.8	2.79	
C0134-6828	052-06	1 34	31.3	-68 28 36	296.7	-48.3	109.7	-39.0	7	3	15.9	3.25	
C0112-6825	052-08	1 12	45.8	-68 25 07	299.6	-48.7	157.2	13.0	7	1	15.9	2.57	
C0117-6848	052-10	1 17	06.3	-68 48 08	299.1	-48.3	119.2	-26.6	7	3	15.0	3.60	
C0121-6923	052-12	1 21	45.9	-69 23 49	298.7	-47.6	136.2	-12.0	6	1	15.9	4.11	
C0110-6932	052-13	1 10	46.9	-69 32 52	300.1	-47.6	132.9	-13.5	6	1	15.9	3.14	
C0127-6842	052-14	1 27	15.2	-69 42 26	298.1	-47.2	209.3	59.2	7	1	15.8	2.65	
C0132-6956	052-16	1 32	30.0	-69 56 22	297.5	-46.9	98.8	-52.7	7	1	15.6	3.97	
C0110-6957	052-17	1 10	02.4	-69 57 05	300.3	-47.2	158.0	10.7	4	1	16.6	3.12	faint sp.
C0120-7028	052-22	1 20	18.1	-70 28 10	299.1	-46.6	147.4	-2.9	7	1	16.6	3.44	
C0109-7022	052-23	1 09	41.4	-70 22 02	300.4	-46.8	114.6	-33.5	7	1	15.4	4.49	
C0124-7056	052-29	1 24	32.4	-70 56 00	298.8	-46.1	108.4	-43.6	7	1	14.9	2.71	
C0116-7058	052-30	1 16	15.5	-70 58 53	298.1	-44.2	168.2	10.4	7	1	15.5	2.77	
C0125-7121	052-31	1 25	14.9	-71 21 24	299.0	-45.7	97.5	-55.3	7	1	15.4	3.08	
C0123-7137	052-33	1 23	00.4	-71 37 09	299.1	-45.4	109.2	-44.2	7	1	15.2	2.98	
C0144-7145	052-35	1 44	25.3	-71 45 28	296.9	-44.9	132.1	-25.4	7	1	14.2	2.90	
C0124-7146	052-36	1 24	45.0	-71 46 17	299.0	-45.3	120.9	-32.9	7	1	15.3	2.70	
C0117-7143	052-37	1 17	40.0	-71 43 13	299.7	-45.4	102.5	-50.1	7	1	15.1	3.04	
C0123-7148	052-38	1 23	27.5	-71 48 03	299.1	-45.2	120.4	-33.5	7	1	15.9	2.89	
C0132-7205	052-39	1 32	39.5	-72 05 06	298.2	-44.8	169.8	13.6	7	1	15.6	2.97	
C0131-7211	052-41	1 31	18.8	-72 11 53	298.4	-44.7	118.9	-37.2	7	1	15.3	2.90	
C0148-7213	052-42	1 48	38.2	-72 13 54	296.6	-44.3	116.8	-42.6	7	1	15.0	3.70	
C0120-7234	052-45	1 20	03.7	-72 34 33	299.7	-44.5	118.0	-36.9	7	1	15.8	4.15	
C0154-7238	052-46	1 54	11.8	-72 38 54	296.3	-43.8	127.3	-33.7	7	1	15.2	2.81	
C0118-7246	052-49	1 18	52.9	-72 46 05	299.8	-44.4	132.2	-22.8	7	1	15.3	3.45	
C0228-7045	053-3	2 28	51.0	-70 45 25	291.7	-44.4	162.8	-1.3	7	4	15.1	2.94	
C0108-6743	080-07	1 08	28.3	-67 43 46	300.1	-49.5	130.9	-10.5	7	1	17.1	3.44	
RAW-1694		1 18	39.1	-72 58 46	300.0	-44.1	173.1	17.6	7	1	17.1		
RAW-1695		1 18	42.9	-72 41 31	299.9	-44.4	149.4	-5.4	7	1	16.9		
RAW-1696		1 18	52.9	-72 46 06	299.9	-44.3	142.9	-12.2	7	1	16.4		

Table 1—Continued

Name	id field	RA	(1950)	Dec	ℓ	b	v_{helio}	v_{gc}	Q	n	R	$B_j - R$	comments
RAW-1704		1 20	30.3 -72 58 26		299.7	-44.1	162.4	6.4	7	1	17.3		
RAW-1705		1 20	57.5 -72 57 00		299.7	-44.1	119.0	-36.9	7	1	16.3		
RAW-1706		1 21	14.0 -73 01 41		299.7	-44.1	160.5	4.5	7	1	16.3		
RAW-1707		1 21	55.6 -73 21 58		299.7	-43.7	124.3	-32.5	7	1	16.5		

REFERENCES

- Arp, H. 1996 *Atlas of Peculiar Galaxies* (Pasadena: California Institute of Technology)
- Da Costa, G.S., & Hatzidimitriou, D. 1998, AJ, 115, 1934
- Davies, R.D., & Wright, A.E. 1977 MNRAS, 180, 71
- Demers, S., & Irwin, M.J. 1991 A&AS, 91, 191
- Demers, S., & Battinelli, P. 1998 AJ, 115, 154
- Demers, S., Irwin, M.J., & Kunkel, W.E. 1993 MNRAS, 260, 103 (Paper I)
- Feitzinger, J.V., Isserstedt, J. & Schmidt-Kaler, Th. 1977 A&A, 57, 265
- Feitzinger, J.V. Space Sci. Rev. 27, 35
- Fujimoto, M., & Sofue, Y. 1976 A&A, 47, 263
- Fujimoto, M., & Sofue, Y. 1977 A&A, 61, 199
- Gardiner, L. T. and Noguchi, M. 1996 MNRAS, 278, 191
- Grondin, L., Demers, S. & Kunkel, W.E. 1992 AJ, 103, 1234
- Hardy, E., Suntzeff, N. B., & Azzopardi, M. 1989 ApJ, 344, 210
- Hatzidimitriou, D., & Hawkins, M.R.S. 1989 MNRAS, 241, 667
- Hatzidimitriou, D., Cannon, R.D., & Hawkins, M.R.S. 1993 MNRAS, 261, 87
- Hatzidimitriou, D., Croke, B.F., Morgan, D.H., & Cannon, R.D. 1997 A&AS, 122, 507
- Hatzidimitriou, D. 1998 in I.A.U. Symposium 190 New Views of the Magellanic Clouds eds. Y.-H. Chu, J.E. Hesser, & N.B. Suntzeff ASP Conf. Series, in press
- Hughes, S.M.G., Wood, P.R., & Reid, N. 1991 AJ, 101, 1304
- Irwin, M. J., Demers, S. & Kunkel, W. E. 1996, BAAS, 28, 931
- Jones, B.F., Klemola A.R., & Lin, D.N.C. 1994 AJ, 107, 1333
- Kendall, M.G., & Stuart, A. 1961 *The Advanced Theory of Statistics* (London, Griffin) Vol.2, p.452.
- Kunkel, W.E. 1980 I.A.U. Symposium 85, Star Clusters ed. J.E. Hesser (Dordrecht: Reidel) p.353
- Kunkel, W. E. 1979 ApJ, 228, 718
- Kunkel, W.E., & Demers, S. 1976 Royal Greenwich Obs. Bull No.182, 241

- Kunkel, W.E., Demers, S., & Irwin M.J. 1995 Third CTIO/ESO Workshop on The Local Group: Comparative and Local Properties, ESO Conference and Workshop Proceedings No.51. Eds.: A Layden, R.C. Smith, & J. Strom (E.S.O., Garching), p.200
- Kunkel, W.E., Demers, S., & Irwin, M.J. 1997 A&AS, 122, 463 (Paper II)
- Kunkel, W.E., Demers, S., Irwin, M.J. & Albert, L. 1997b Ap.J. 488, L129 (Paper III)
- Lee, M.G., Kim, E., & Geisler, D. 1997 AJ, 114, 1824
- Lin, D.N.C., & Lynden-Bell, D. 1977 MNRAS, 181, 37
- Lynden-Bell, D. 1976 Royal Greenwich Obs. Bull No.182, 235
- Mateo, M., & Hatzidimitriou, D. 1992 I.A.U. Symposium 149, The Stellar Populations of Galaxies, eds.: B. Barbuy & A. Renzini (Kluwer: Dordrecht), p.454
- Mathewson, D.S., Schwarz, M.P., & Murray, J.D. 1977 ApJ, 217, L5
- Mathewson, D.S., & Ford, V.L. 1984 in I.A.U. Symposium 108 Structure and Evolution of the Magellanic Clouds eds. S. van den Bergh & K.S. de Boer (Dordrecht: Reidel) p.125
- Mathewson, D.S., Ford, V.L., & Visvanathan, N. 1986 ApJ, 301, 664
- Mathewson, D.S., Wayte, S.R., Ford, V.L., & Ruan, K. 1987 Proc. A. S. Austr., 7, 19
- Mathewson, D.S., Ford, V.L., and Visvanathan, N. 1988 ApJ, 333, 617
- Maurice, E., Martin, N., & Bouchet, P. 1989 A&AS, 78, 445
- McClure, R.D., Fletcher, J.M., Grundman W.A., & Richardson, E.H. 1985 in I.A.U. Colloquium No.88 Stellar Radial Velocities eds. A.G.D. Philip & D.W. Latham (New York, L.Davis Press), p.49
- McGee, R., & Newton, L. 1986 Proc. A.S. Austr., 6, 471
- Merritt, D., 1996 AJ, 111, 2462
- Moore, B., & Davis, M. 1994 MNRAS, 270, 209
- Murai, T., & Fujimoto, M. 1980 PASJ, 32, 581
- Odewahn, S. C. 1994 AJ, 104, 1320
- Olszewski, E.O., Schommer, R.A., Suntzeff, N.B., & Harris, H.C. 1991 AJ, 101, 515
- Patterson, R.J., & Thuan, T.X. 1993 ApJ, 400, L55
- Putnam, M.E., Gibson, B.K., & Staveland-Smith, L. 1998 I.A.U. Symposium 190 New Views of the Magellanic Clouds eds. Y.-H. Chu, J.E. Hesser, & N.B. Suntzeff ASP Conf Series, in press

- Sancisi, R., Thonnard, N., and Ekers, R.D. 1987 ApJ, 315, L42
- Toomre, A., & Toomre, Y. 1972 ApJ, 178, 623
- Totten, E.J. & Irwin, M.J. 1998 MNRAS, 294, 1
- Wannier, P., & Wrixon, G.T. 1972 ApJ, 119, L119
- Weiner, B. J., & Williams, T. B. 1996, AJ, 111, 1156
- Welch, D. L. I.A.U. Symposium 190 New Views of the Magellanic Clouds eds. Y.-H. Chu, J.E. Hesser, and N.B. Suntzeff ASP Conf Series, in press
- Welch, D.L., McLaren, R.A., Madore, B.F., & McAlary, C.W. 1987 ApJ, 321, 162
- Westerlund, B.E. & Glaspey, J. 1971 A&A, 10, 1